Alexander V. Skripov*, Kai Volgmann, C. Vinod Chandran, Roman V. Skoryunov, Olga A. Babanova, Alexei V. Soloninin, Shin-ichi Orimo and Paul Heitjans

NMR Studies of Lithium Diffusion in Li$_3$(NH$_2$)$_2$I Over Wide Range of Li$^+$ Jump Rates

Abstract: We have studied the Li diffusion in the complex hydride Li$_3$(NH$_2$)$_2$I which appears to exhibit fast Li ion conduction. To get a detailed insight into the Li motion, we have applied ^{7}Li nuclear magnetic resonance spectroscopy methods, such as spin-lattice relaxation in the laboratory and rotating frames of reference, as well as spin-alignment echo. This combined approach allows us to probe Li jump rates over the wide dynamic range ($\sim 10^2$–10^9 s^{-1}). The spin-lattice relaxation data in the range 210–410 K can be interpreted in terms of a thermally-activated Li jump process with a certain distribution of activation energies. However, the low-temperature spin-alignment echo decays at $T \leq 200$ K suggest the presence of another Li jump process with the very low effective activation energy.

Keywords: complex hydride; ion diffusion; nuclear magnetic resonance; spin-alignment echo; spin-lattice relaxation.

1 Introduction

Complex hydrides showing fast ionic conductivity have attracted much recent attention as potential solid electrolytes [1–3]. These compounds form ionic crystals consisting of metal cations and complex anions, such as [BH$_4$]$^-$, [NH$_2$]$^-$, [AlH$_6$]$^{3-}$, [B$_{12}$H$_{12}$]$^{2-}$, [B$_{10}$H$_{10}$]$^{2-}$, and [CB$_9$H$_{10}$]$^-$. Since the discovery of high Li$^+$-ion

Corresponding author: Alexander V. Skripov, Institute of Metal Physics, Ural Branch of the Russian Academy of Sciences, S. Kovalevskoi 18, Ekaterinburg 620990, Russia, e-mail: skripov@imp.uran.ru
Kai Volgmann, C. Vinod Chandran and Paul Heitjans: Institut für Physikalische Chemie und Elektrochemie, Leibniz Universität Hannover, Callinstr. 3-3a, Hannover 30167, Germany
Roman V. Skoryunov, Olga A. Babanova and Alexei V. Soloninin: Institute of Metal Physics, Ural Branch of the Russian Academy of Sciences, S. Kovalevskoi 18, Ekaterinburg 620990, Russia
Shin-ichi Orimo: Institute for Materials Research, Tohoku University, Sendai 980-8577, Japan; and WPI-Advanced Institute for Materials Research, Tohoku University, Sendai 980-8577, Japan

conductivity in the hexagonal phase of $LiBH_4$ [4], the family of complex hydrides with superionic-conduction properties have been steadily growing. Examples of the complex hydrides with high Li^+- or Na^+-ion conductivity include $LiBH_4$-LiX solid solutions (X = Cl, Br, I) [5], $Li_2(BH_4)(NH_2)$ [6], $Na_2(BH_4)(NH_2)$ [2], Li_2NH [7], $LiR(BH_4)_3Cl$ (R = La, Ce, Gd) [8, 9], $Na_2B_{12}H_{12}$ [10], $Na_2B_{10}H_{10}$ [11], $LiCB_9H_{10}$ and $NaCB_9H_{10}$ [12]. Recent studies [13] have revealed that the room-temperature ionic conductivity of the solid-solution $Na_2(CB_9H_{10})(CB_{11}H_{12})$ is higher than that of any other known solid Na^+ or Li^+ conductor. Apart from prospective practical applications, complex hydrides are of interest as model systems for studies of the mechanisms of cation diffusion. Indeed, complex anions are known to exhibit a rotational (reorientational) motion, and this localized motion may affect the translational diffusion of cations [14, 15].

Studies of the anion substitutions in the $LiNH_2$–LiI system [16] have found the mixed-anion complex hydride $Li_3(NH_2)_2I$ with the Li^+ conductivity of 1.7×10^{-5} S/cm at 300 K, which is several orders of magnitude higher than the conductivity of both $LiNH_2$ and LiI. The double-layered crystal structure of $Li_3(NH_2)_2I$ is hexagonal (space group $P6_3mc$) [16]; it has two crystallographically inequivalent Li sites, both of them are fully occupied. Nuclear magnetic resonance (NMR) spectroscopy has proved to be an effective technique for studies of atomic motion in solids (including both translational diffusion and reorientations) at the microscopic level [17, 18]. Previous ^7Li and ^1H NMR measurements of the spectra and spin-lattice relaxation rates in $Li_3(NH_2)_2I$ [19] have revealed the fast translational diffusion of Li^+ ions with the characteristic jump rate reaching ~10^8 s^{-1} at 310 K. In that work, the Li^+ diffusion parameters were evaluated on the basis of the model description of the temperature-dependent ^7Li spin-lattice relaxation rate measured at the resonance frequencies of 14 and 28 MHz [19]. The drawback of such an approach is that Li^+ jump rates are probed over a limited dynamic range. In order to increase the frequency range over which the atomic jump dynamics can be probed, it is useful to combine the low-field and high-field spin-lattice relaxation measurements with the rotating-frame spin relaxation measurements [20, 21] and the spin-alignment echo (SAE) NMR spectroscopy [22–26]. Such a combined NMR approach allows one to trace Li diffusion over a very wide dynamic range (up to 10 orders of magnitude) [27]. In the present work, we apply ^7Li NMR measurements of the high-field spin-lattice relaxation rate, the rotating-frame spin-lattice relaxation rate, and SAE NMR to study Li jump motion in the complex hydride $Li_3(NH_2)_2I$ over a wide jump-rate range. This is the first application of the SAE NMR technique to a complex hydride system with high ionic conductivity. The results are compared with those of previous low-field spin-lattice relaxation measurements [19], and the mechanism of Li diffusion in $Li_3(NH_2)_2I$ is discussed on the basis of all available experimental data.

2 Experimental

The sample preparation was analogous to that described earlier [16]. All preparation and manipulation procedures were performed in a glove-box filled with purified argon. The LiNH$_2$–LiI mixture (3:1 molar ratio) was mechanically milled for 5 h in an argon atmosphere using a planetary Fritsch 7 ball mill at 400 rpm. After the milling, the sample was heat-treated at 423 K for 12 h under argon. According to X-ray diffraction analysis, the major phase of resulting sample was the hexagonal Li$_3$(NH$_2$)$_2$I compound [space group $P6_3mc$, $a = 7.09109(5)$ Å, $c = 11.50958(10)$ Å]. The sample also contained unreacted LiNH$_2$ as a minor phase. For NMR experiments, the sample was flame-sealed in a glass tube under vacuum.

NMR measurements were performed on a Bruker Avance III 600 pulse spectrometer at the ^{7}Li resonance frequency $\omega/2\pi = 233.3$ MHz. A commercial single-resonance broadband NMR probe was used. The sample temperature was regulated by heating or cooling a flow of N$_2$ gas. Measurements were carried out in the temperature range of 164–410 K. The nuclear spin-lattice relaxation rates were measured using the saturation – recovery method. The spin-lattice relaxation rates in the rotating frame of reference were measured using the spin-locking frequency of 10 kHz. The decay of the spin-alignment echoes was monitored using the Jeener–Broekaert pulse sequence [28],

$$(\pi/2)_x - t_p - (\pi/4)_y - t_m - (\pi/4)_\varphi - \text{acquisition}.$$

In our experiments, the preparation time t_p of 20 μs was kept constant, while the mixing time t_m was varied between 1 μs and 10 s.

3 Results and discussion

Measurements of the ^{7}Li spin-lattice relaxation rate R_1 in the temperature range 330–410 K have shown that the recovery of nuclear spin magnetization in Li$_3$(NH$_2$)$_2$I is single-exponential. The temperature dependence of R_1 exhibits a maximum near 375 K. Such a maximum is typical of the case of spin-lattice relaxation due to atomic motion [29]; it is expected to occur at the temperature at which the atomic jump rate $\tau^{-1}(T)$ becomes nearly equal to the resonance frequency ω, i.e. when $\omega\tau \approx 1$.
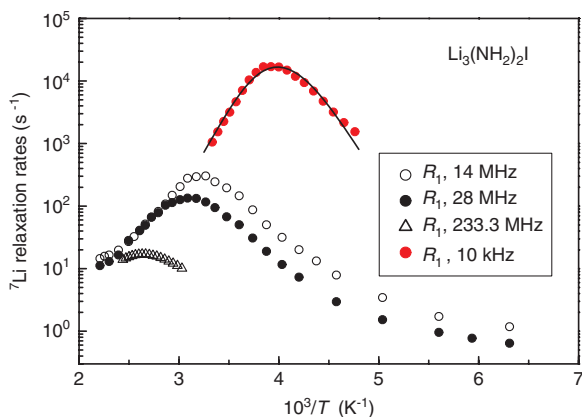
Measurements of the rotating-frame spin-lattice relaxation rate $R_{1\rho}$ in the temperature range 210–300 K have revealed slight deviations from the single-exponential decay of the free-induction signal as a function of the spin-locking pulse length. This decay can be reasonably approximated by the stretched-exponential

function $\exp[-(tR_{1\rho})^\beta]$ with $\beta \approx 0.9$ over the entire temperature range studied. The temperature dependence of $R_{1\rho}$ is found to have a maximum near 250 K; this maximum corresponds to the condition $\omega_1 \tau \approx 1$, where $\omega_1 = \gamma_{Li} B_1$, γ_{Li} is the ^{7}Li gyromagnetic ratio, and B_1 is the amplitude of the rf magnetic field. Since ω_1 is much lower than the resonance frequency ω, the $R_{1\rho}(T)$ maximum is observed at a considerably lower temperature than the $R_1(T)$ maximum.

Figure 1 combines the results of the present $R_1(T)$ and $R_{1\rho}(T)$ measurements and the results of our previous $R_1(T)$ measurements [19] at low resonance frequencies (14 and 28 MHz) for $Li_3(NH_2)_2I$. The relaxation rates are shown at the logarithmic scale as functions of the inverse temperature. According to the standard theory of nuclear spin-lattice relaxation due to atomic motion [29], in the limit of slow motion ($\omega\tau \gg 1$), R_1 should be proportional to $\omega^{-2}\tau^{-1}$, and in the limit of fast motion ($\omega\tau \ll 1$), R_1 should be proportional to τ and frequency-independent. These predictions correspond to three-dimensional diffusion, which is the case of Li jump motion in $Li_3(NH_2)_2I$ [19]. If the temperature dependence of the jump rate τ^{-1} for Li diffusion is described by the Arrhenius law with the activation energy E_a,

$$\tau^{-1} = \tau_0^{-1}\exp(-E_a / k_B T), \tag{1}$$

a plot of $\ln R_1$ vs. T^{-1} should be linear in the limits of both slow and fast motion with the slopes of $-E_a/k_B$ and E_a/k_B, respectively. The same also applies to the plot of $\ln R_{1\rho}$ vs. T^{-1} in the region of the $R_{1\rho}(T)$ peak. However, as can be seen from Figure 1, the observed high-temperature slope of this plot is steeper than the


Fig. 1: ^{7}Li spin-lattice relaxation rates R_1 measured at different resonance frequencies and the rotating-frame spin-lattice relaxation rates $R_{1\rho}$ for $Li_3(NH_2)_2I$ as functions of inverse temperature. The solid line shows the fit of the model with a Gaussian distribution of the activation energies to the $R_{1\rho}$ data.

low-temperature one. This feature suggests the presence of a certain distribution of τ^{-1} values [30]. Such a distribution in Li$_3$(NH$_2$)$_2$I can be expected, since Li ions in this compound occupy two types of sites with slightly different local environments. The simplest approach taking into account a jump rate distribution is based on the model with a Gaussian distribution of the activation energies [30]. A similar approach was used earlier for analysis of the low-frequency R_1 data in Li$_3$(NH$_2$)$_2$I [19]. The parameters of this model are the average activation energy $\bar{E}_a$, the distribution width (dispersion) ΔE_a, and the pre-exponential factor τ_0 in the Arrhenius law. The solid curve in Figure 1 shows the results of the fit of this model to the $R_{1\rho}(T)$ data; the corresponding motional parameters are $\bar{E}_a = 0.53$ eV, $\Delta E_a = 0.024$ eV, and $\tau_0 = 1.7 \times 10^{-16}$ s. Note that the value of $\bar{E}_a$ found from the $R_{1\rho}(T)$ fit is considerably higher than that derived from the low-frequency $R_1(T)$ fits (0.38 eV) [19]. This difference can be ascribed to the fact that, due to the large amplitude of the $R_{1\rho}(T)$ peak, it is less sensitive to background contributions [27] to the nuclear spin relaxation rate, as compared to the $R_1(T)$ peak. As it has been shown previously [19], the observed deviations of the low-frequency $R_1(T)$ data from the Arrhenius behavior at high temperatures ($T > 400$ K) accompanied by the reappearance of a certain frequency dependence can be attributed to the motion of [NH$_2$]$^-$ anions. The 'model-independent' approach to interpretation of different relaxation rates will be discussed below.

The spin-alignment echo measurements have been used to probe Li jumps with $\tau^{-1} < 10^4$ s^{-1}. Since the sharp narrowing of the ^{7}Li NMR spectrum in Li$_3$(NH$_2$)$_2$I [19] occurs near 210 K, the SAE-NMR measurements were performed at temperatures below this narrowing region (in the range 164–200 K). Figure 2 shows the decays of the normalized spin-alignment echo amplitudes A_2 as functions of the mixing time t_m at the temperatures of 164, 180, and 200 K. A similar shape of the SAE decay is observed at $T = 190$ K. The decays have been satisfactorily described by the stretched exponential function,

$$A_2(t_m) = A_0 \exp[-(t_m / \tau_{SAE})^\gamma], \tag{2}$$

where the stretching exponent γ is in the range of 0.42–0.46 for all the temperatures studied, and τ_{SAE} can be identified as the motional correlation time of the Li jump process. It should be noted that in some ionic conductors, the SAE decay exhibits two-step behavior with an intermediate plateau [27]. The second 'step' may appear due to the effects of spin-lattice relaxation on the echo amplitude. In the case of Li$_3$(NH$_2$)$_2$I, such a plateau amplitude appears to be close to zero, which is consistent with multiple jump possibilities for Li ions [27]. Furthermore, the absence of the effects of spin-lattice relaxation on the SAE decay can be considered as a proof that this decay is not affected by any non-diffusive
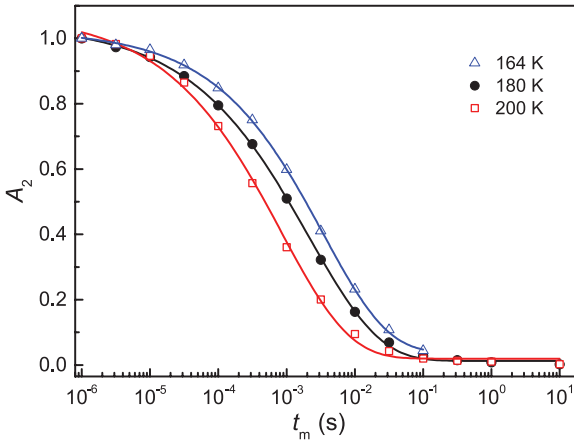
Fig. 2: Decays of normalized ^{7}Li spin-alignment echo amplitudes for Li$_3$(NH$_2$)$_2$I at 164, 180 and 200 K as functions of the mixing time t_m. The lines show the fits of the stretched-exponential function [Eq. (2)] to the data.

contributions. Thus, we can conclude that the measured values of $(\tau_{SAE})^{-1}$ indeed reflect the jump rates.

In Figure 3, the Li jump rates derived from the SAE-NMR measurements are shown together with those obtained from the R_1 maxima at different resonance
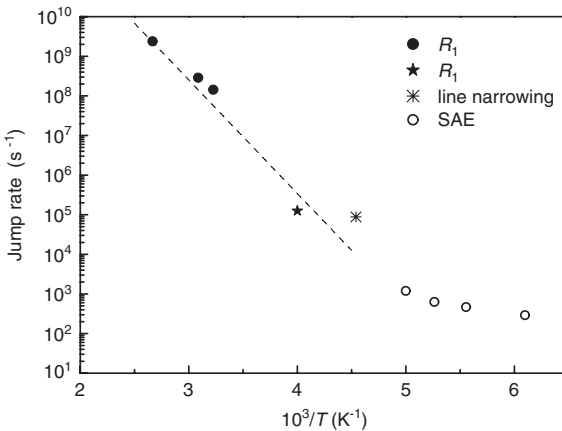

Fig. 3: Li jump rates in Li$_3$(NH$_2$)$_2$I derived from the $R_1(T)$ and $R_{1\rho}(T)$ maxima and from the spin-alignment echo measurements. The dashed line corresponds to the Arrhenius law with the activation energy of 0.56 eV. An estimate of the jump rate from the narrowing of the ^{7}Li NMR line [19] is also included.

frequencies and from the $R_{1\rho}$ maximum. The τ^{-1} values from the relaxation rate data are determined on the basis of the maximum conditions $\omega\tau = 0.616$ and $\omega_1\tau = 0.5$ for the R_1 and $R_{1\rho}$ peaks, respectively. It should be noted that the positions of the $R_1(T)$ and $R_{1\rho}(T)$ maxima remain practically unchanged in the presence of distributions of the activation energies [30]. Thus, Figure 3 can be considered as a 'model-independent' Arrhenius plot of the jump rates over a wide frequency range. Included in Figure 3 is also a rough estimate of the jump rate from the narrowing of the ^{7}Li NMR line [19]; this estimate gives $\tau^{-1} \approx 9 \times 10^4$ s^{-1} at 220 K. The points in this figure resulting from the R_1 and $R_{1\rho}$ data appear to represent a single thermally-activated process of Li$^+$ diffusion. The dashed line in Figure 3 corresponds to the Arrhenius law with the activation energy of 0.56 eV; this value is close to the average activation energy derived from the model description of the $R_{1\rho}(T)$ data. It should be noted that in cases when the dipolar interaction with paramagnetic centers provides an important contribution to the relaxation rate, the $R_{1\rho}(T)$ maximum is determined by the condition $\omega_{1eff}\tau \approx 0.5$, where the effective locking frequency ω_{1eff} is larger than ω_1, since the effective locking field is the sum of the field B_1 resulting from the rf pulse and the local field B_{local} [31]. Taking this possibility into account would lead to an upper shift of the $R_{1\rho}$ point in Figure 3. It is evident, however, that the behavior of τ_{SAE} in the temperature range 164–200 K cannot be described in terms of the same thermally-activated process. The temperature dependence of τ_{SAE} in this range suggests the presence of another Li jump process with low activation energy. It is interesting to note that the low-frequency $R_1(T)$ data also exhibit a change in the slope below 200 K (see Figure 1). However, for the spin-lattice relaxation, it is difficult to distinguish between a real change in the activation energy and a background contribution to the relaxation rate.

On the basis of proton NMR data, it has been concluded [19] that at $T < 400$ K, Li jump motion in Li$_3$(NH$_2$) is not affected by reorientations of NH$_2$ groups. It seems more probable that high Li mobility in this compound is related to its structural features. The schematic view of the crystal structure of Li$_3$(NH$_2$)$_2$I is shown in Figure 4. Crystallographically inequivalent Li sites (Li1 and Li2) form alternating layers perpendicular to the c axis. The sublattice of Li sites is characterized by rather short Li–Li distances. Each Li1 atom has two Li1 nearest neighbors (in the same layer) at a distance of 2.28 Å and one Li2 nearest neighbor (in the adjacent layer) at a distance of 2.39 Å. Each Li2 has one Li1 nearest neighbor (in the adjacent layer) at a distance of 2.39 Å and two Li2 nearest neighbors (in the same layer) at a distance of 2.84 Å. According to the structural studies [16], both Li1 and Li2 sites are fully occupied; therefore, interstitial sites in the lattice may play an important role for Li$^+$ diffusion. As can be seen from Figure 4, each Li atom is tetrahedrally coordinated by three N atoms and one I atom, and these N$_3$I tetrahedra share edges or vertices. Between the N$_3$I tetrahedra, there are rather
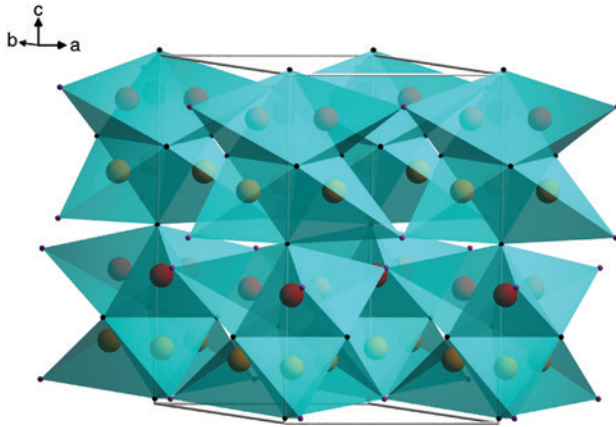
Fig. 4: Schematic view of the structure of $Li_3(NH_2)_2I$ with N_3I tetrahedra coordinating each Li site. Red spheres: Li1 sites; orange spheres: Li2 sites; small black spheres: N sites; and small violet spheres: I sites. H sites are omitted for clarity.
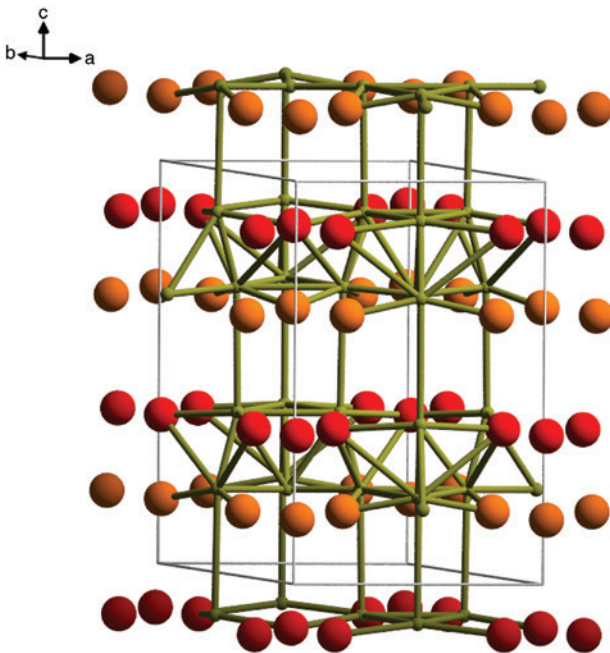
Fig. 5: The sublattice of Li sites in $Li_3(NH_2)_2I$ and the network of channels for Li^+ diffusion. Red spheres: Li1 sites; orange spheres: Li2 sites; and olive spheres: large interstitial sites. The olive bars show the possible diffusion paths.

large voids (interstitial sites), which can be reached by Li$^+$ via jumps through the faces of the tetrahedra. Possible diffusion paths accessible to Li$^+$ ions have been analyzed using the program TOPOS [32]. The analysis has revealed three types of large interstitial sites (2*b* and two types of 6*c* sites) located slightly off the Li layers; the effective radii of these voids are in the range 1.58–1.70 Å. These interstitial sites form the three-dimensional network of channels shown in Figure 5. The corresponding effective radii of the channels are in the range 2.11–2.46 Å; therefore, this network represents possible paths for Li$^+$ diffusion. It is reasonable to assume that the low-temperature jump process revealed by SAE measurements may be related to some kind of localized motion between the regular Li sites and the nearest interstitial sites.

4 Conclusions

Lithium jump rates in the complex hydride Li$_3$(NH$_2$)$_2$I have been probed over a wide dynamic range (~10^2–10^9 s^{-1}) using different NMR techniques. The results of ^{7}Li NMR measurements of the spin-lattice relaxation rates in both the laboratory and rotating frame of reference can be satisfactorily described in terms of the model with a Gaussian distribution of the activation energies for Li jump motion. In particular, the temperature dependence of the rotating-frame spin-lattice relaxation rates in Li$_3$(NH$_2$)$_2$I is reasonably described by the average activation energy of 0.53 eV. This value is also close to the activation energy resulting from the 'model-independent' analysis based on the relaxation rate maxima at different frequencies. However, the results of ^{7}Li spin-alignment echo measurements of ultraslow Li motion at $T \leq 200$ K do not follow the Arrhenius law describing the high-temperature jump rates. These results suggest the presence of an additional low-temperature Li jump process with a very low effective activation energy.

References

1. M. Matsuo, S. Orimo, Adv. Energy Mater. **1** (2011) 161.
2. M. Matsuo, S. Kuromoto, S. Sato, H. Oguchi, H. Takamura, S. Orimo, Appl. Phys. Lett. **100** (2012) 203904.
3. P. E. de Jongh, D. Blanchard, M. Matsuo, T. J. Udovic, S. Orimo, Appl. Phys. A Mater. Sci. Process. **122** (2016) 1.
4. M. Matsuo, Y. Nakamori, S. Orimo, H. Maekawa, H. Takamura, Appl. Phys. Lett. **91** (2007) 224103.
5. H. Maekawa, M. Matsuo, H. Takamura, M. Ando, Y. Noda, T. Karahashi, S. Orimo, J. Am. Chem. Soc. **131** (2009) 894.
6. M. Matsuo, A. Remhof, P. Martelli, R. Caputo, M. Ernst, Y. Miura, T. Sato, H. Oguchi, H. Maekawa, H. Takamura, A. Borgschulte, A. Züttel, S. Orimo, J. Am. Chem. Soc. **131** (2009) 16389.
7. B. A. Boukamp, R. A. Huggins, Phys. Lett. A **72** (1979) 464.
8. M. B. Ley, D. B. Ravnsbæk, Y. Filinchuk, Y. S. Lee, R. Janot, Y. W. Cho, J. Skibsted, T. R. Jensen, Chem. Mater. **24** (2012) 1654.
9. M. B. Ley, S. Boulineau, R. Janot, Y. Filinchuk, T. R. Jensen, J. Phys. Chem. C **116** (2012) 21267.
10. T. J. Udovic, M. Matsuo, A. Unemoto, N. Verdal, V. Stavila, A. V. Skripov, J. J. Rush, H. Takamura, S. Orimo, Chem. Commun. **50** (2014) 3750.
11. T. J. Udovic, M. Matsuo, W. S. Tang, H. Wu, V. Stavila, A. V. Soloninin, R. V. Skoryunov, O. A. Babanova, A. V. Skripov, J. J. Rush, A. Unemoto, H. Takamura, S. Orimo, Adv. Mater. **26** (2014) 7622.
12. W. S. Tang, M. Matsuo, H. Wu, V. Stavila, W. Zhou, A. Talin, A. V. Soloninin, R. V. Skoryunov, O. A. Babanova, A. V. Skripov, A. Unemoto, S. Orimo, T. J. Udovic, Adv. Energy Mater. **6** (2016) 1502237.
13. W. S. Tang, K. Yoshida, A. V. Soloninin, R. V. Skoryunov, O. A. Babanova, A. V. Skripov, M. Dimitrievska, V. Stavila, S. Orimo, T. J. Udovic, ACS Energy Lett. **1** (2016) 659.
14. A. V. Skripov, A. V. Soloninin, M. B. Ley, T. R. Jensen, Y. Filinchuk, J. Phys. Chem. C **117** (2013) 14965.
15. Y. S. Lee, M. B. Ley, T. R. Jensen, Y. W. Cho, J. Phys. Chem. C **120** (2016) 19035.
16. M. Matsuo, T. Sato, Y. Miura, H. Oguchi, Y. Zhou, H. Maekawa, H. Takamura, S. Orimo, Chem. Mater. **22** (2010) 2702.
17. A. V. Skripov, A. V. Soloninin, O. A. Babanova, R. V. Skoryunov, J. Alloys Compd. **645** (2015) S428.
18. C. Vinod Chandran, P. Heitjans, Ann. Rep. NMR Spectrosc. **89** (2016) 1.
19. A. V. Skripov, R. V. Skoryunov, A. V. Soloninin, O. A. Babanova, M. Matsuo, S. Orimo, J. Phys. Chem. C **119** (2015) 13459.
20. D. C. Look, I. J. Lowe, J. Chem. Phys. **44** (1966) 2995.
21. D. C. Ailion, C. P. Slichter, Phys. Rev. **137** (1965) A235.
22. H. W. Spiess, J. Chem. Phys. **72** (1980) 6755.
23. R. Böhmer, T. Jörg, F. Qi, A. Titze, Chem. Phys. Lett. **316** (2000) 419.
24. F. Qi, C. Rier, R. Böhmer, W. Franke, P. Heitjans, Phys. Rev. B **72** (2005) 104301.
25. M. Wilkening, P. Heitjans, Solid State Ionics **177** (2006) 3031.
26. M. Wilkening, P. Heitjans, ChemPhysChem **13** (2012) 53.

27. M. Wilkening, P. Heitjans, Phys. Rev. B **77** (2008) 024311.
28. J. Jeener, P. Broekaert, Phys. Rev. **157** (1967) 232.
29. A. Abragam, The Principles of Nuclear Magnetism, Clarendon Press, Oxford (1961).
30. J. T. Markert, E. J. Cotts, R. M. Cotts, Phys. Rev. B **37** (1988) 6446.
31. A. Kuhn, M. Kunze, P. Sreeraj, H.-D. Wiemhöfer, V. Thangadurai, M. Wilkening, P. Heitjans, Solid State Nucl. Magn. Reson. **42** (2012) 2.
32. V. A. Blatov, A. P. Shevchenko, D. M. Proserpio, Cryst. Growth Des. **14** (2014) 3576.